

Article

Effects of Cu Addition on Mechanical Behaviour, Microstructural Evolution and Anti-Corrosion Performance of TiAl-Based Intermetallic Alloy under Different Strain Rates

Cheng-Hsien Kuo ¹, Tao-Hsing Chen ^{2,*} and Ting-Yang Zeng ²

¹ Department of Mold and Die Engineering, National Kaohsiung University of Science and Technology, Kaohsiung 80778, Taiwan; chuckkuo@nkust.edu.tw

² Department of Mechanical Engineering, National Kaohsiung University of Science and Technology, Kaohsiung 80778, Taiwan; stars0619@yahoo.com.tw

* Correspondence: thchen@nkust.edu.tw; Tel.: +886-7-3814526 (ext. 15330)

Abstract: TiAl-based intermetallic alloys are prepared with Cu concentrations of 3–5 at.% (atomic ratio). The mechanical properties and microstructural characteristics of the alloys are investigated under static and dynamic loading conditions using a material testing system (MTS) and split-Hopkinson Pressure Bar (SHPB), respectively. The electrochemical properties of the various alloys are then tested in Ringer's solution. It is shown that the level of Cu addition significantly affects both the flow stress and the ductility of the samples. For Cu contents of 3 and 4 at.%, respectively, the flow stress and strain rate sensitivity increase at higher strain rates. Furthermore, for a constant strain rate, a Cu content of 4 at.% leads to an increased fracture strain. However, for the sample with the highest Cu addition of 5 at.%, the flow stress and fracture strain both decrease. The X-ray diffraction (XRD) patterns and optical microscopy (OM) images reveal that the lower ductility is due to the formation of a greater quantity of γ phase in the binary TiAl alloy system. Among all the specimens, that with a Cu addition of 4 at.% has the best anti-corrosion performance. Overall, the results indicate that the favourable properties of the TiAlCu₄ sample stem mainly from the low γ phase content of the microstructure and the high α_2 phase content.

Keywords: TiAl-based intermetallic alloy; strain rate; microstructural evolution; fracture surface



Citation: Kuo, C.-H.; Chen, T.-H.; Zeng, T.-Y. Effects of Cu Addition on Mechanical Behaviour, Microstructural Evolution and Anti-Corrosion Performance of TiAl-Based Intermetallic Alloy under Different Strain Rates. *Materials* **2021**, *14*, 5056. <https://doi.org/10.3390/ma14175056>

Academic Editor: Jan Haubrich

Received: 2 August 2021

Accepted: 2 September 2021

Published: 3 September 2021

Publisher's Note: MDPI stays neutral with regard to jurisdictional claims in published maps and institutional affiliations.



Copyright: © 2021 by the authors. Licensee MDPI, Basel, Switzerland. This article is an open access article distributed under the terms and conditions of the Creative Commons Attribution (CC BY) license (<https://creativecommons.org/licenses/by/4.0/>).

1. Introduction

Intermetallic alloys have attracted significant attention in the literature in recent decades due to their high operational temperatures, good wear resistance, superior hardness, and good electrochemical resistance. Among the many intermetallic alloys which have been developed, titanium aluminium (TiAl) is one of the most widely used in the aerospace and automotive industries due to its light weight and high strength [1,2]. TiAl alloy may exist with two basic microstructures: duplex and lamellar [3]. For both microstructures, the room-temperature ductility and fracture toughness are inversely related. Generally speaking, the creep resistance and fracture toughness of lamellar TiAl alloy are better than those of duplex TiAl alloy under ambient temperatures. However, as the temperature is increased to 800 °C and more [3–5], a sudden and substantial loss in the creep resistance occurs.

The literature contains many attempts to improve the room-temperature ductility and high-temperature strength of lamellar TiAl through the addition of substitutional elements (e.g., Nb and Mo [6–8]), or interstitial elements (e.g., B, C and N [9,10]). Nb and Mo both serve as β -stabilizing elements, and result in the formation of disordered β -phase with a better ductility than α_2 or γ phase at elevated temperatures. Meanwhile, interstitial elements, such as C and N, improve the fracture strain and yield stress. Cu-based TiAl alloys are a promising solution for high-temperature structural applications with high

strength and toughness requirements [11,12]. Moreover, several studies have shown that Cu addition is also beneficial in improving the biocompatibility, corrosion resistance, and ductility of TiAl alloy [13–15].

For many engineering metals and alloys, the flow behaviour under elevated strain rates and temperature conditions is extremely complex. For example, significant work hardening frequently occurs as the strain rate increases [16]. By contrast, a higher temperature usually results in thermal softening [17]. Thus, the flow behaviour of the material is essentially the result of a competition between the effects of work hardening and thermal softening, respectively. It was shown in [18] that the dependence of the flow stress on the strain rate and temperature is associated with the motion of glide dislocations over obstacles in the microstructure. Moreover, under extreme strain rate conditions, the flow response is determined primarily by the effects of viscous drag and/or dislocation generation [19]. The literature contains various constitutive equations for describing the stress–strain response of metals and alloys under different strain rates and temperatures, including the Zerilli-Armstrong and Johnson-Cook models [20–22].

As an alloy deforms, the microstructural evolution is dependent on both the strain rate and the temperature. At higher strain rates, dislocation multiplication occurs more readily and prompts a strengthening effect [23,24]. Conversely, at higher temperatures, dislocation annihilation occurs, which leads to a significant loss in flow resistance [25,26]. Both effects have a major impact on the mechanical properties of the deformed microstructure, and must therefore be carefully considered when attempting to predict the response of metals and alloys in typical service applications.

The quasistatic mechanical response of TiAl intermetallic alloys has attracted considerable attention in the literature [27–29]. However, the effects of high strain rate deformation on the flow behaviour of TiAl alloy are still unclear. Nonetheless, developing such an understanding is essential since high strain rate deformation often results in the generation of adiabatic shear bands, which then prompt crack initiation [30–33]. Accordingly, this study investigates the mechanical properties and microstructural evolution of Cu-based TiAl intermetallic alloy at strain rates in the range of 10^{-3} – $4 \times 10^3 \text{ s}^{-1}$ using a material testing system (MTS) and split-Hopkinson Pressure Bar (SHPB). The experimental tests are performed at room temperature using TiAl specimens with Cu contents of 3–5 at.%, respectively. The electrochemical properties of the various samples are additionally tested under ambient conditions in Ringer's solution over a voltage range of –600 mV to 200 mV.

2. Material Preparation and Experimental Procedures

High-purity (99.99%) Ti, Al and Cu powders were purchased from Golden Optoelectronic Co. Ltd. (Golden, Optoelectronic Co. Ltd, New Taipei city, Taiwan). Cu-based TiAl intermetallic alloys were prepared in a vacuum arc melted furnace back-filled with argon. The specimens contained an Al content of 46 at.%, Cu contents of 3, 4 or 5 at.%, and a balance of Ti. To ensure compositional homogeneity, the specimens were heated at 1473 K for 24 h, allowed to cool to room temperature in the furnace, and then reheated to 1473 K once again. Furthermore, for each specimen, the heating and reheating cycle was performed at least three times. The as-cast circular ingots (with dimensions of 30 mm \times 4 mm) were machined into cylindrical specimens (length: 5 ± 0.1 mm; diameter: 5.1 mm) using an EDM machine and centre-grinding process.

The mechanical properties of the various samples were investigated at room temperature under both quasistatic and dynamic loading conditions. The quasistatic tests were performed at strain rates of 10^{-3} , 10^{-2} and 10^{-1} s^{-1} , respectively, using an MTS 810 testing system (MTS Systems Corporation, Minneapolis, MN, USA). The dynamic tests were performed at strain rates of $3 \times 10^3 \text{ s}^{-1}$, $4 \times 10^3 \text{ s}^{-1}$ and $5 \times 10^3 \text{ s}^{-1}$ using a SHPB system (Advance Instrument Inc. Corporation, Taipei, Taiwan). In performing the dynamic tests, the specimen were lubricated with molybdenum disulphide grease to ensure frictionless conditions, and were placed between the incident bar and transmitter bar of the SHPB system. The incident bar was then launched by a gas gun system. The

resulting stress–strain response of the specimen was evaluated by measuring the stress waves propagating through the SHPB system using strain gauges mounted on the incident and transmitter bars, respectively.

The microstructural properties of the test specimens were observed by scanning electron microscopy (SEM; JSM-7001; JEOL Ltd., Akishima, Japan) and optical microscopy (OM; Metallurgical Microscopy MR5000, Kaohsiung, Taiwan). In addition, the phases of the specimens with different Cu additions were determined via X-ray diffraction and the scattering angle was from 20° to 120° at speed of 1° per minute and the operation voltage of 40 kV with Cu $K\alpha$ radiation (Philips X-ray diffractometer; Spectris plc., Almelo, The Netherlands). Finally, the electrochemical corrosion properties of the samples were examined by electrochemical tests performed in Ringer’s solution (9.0 gL^{-1} NaCl, 0.43 gL^{-1} KCl, 0.24 gL^{-1} CaCl_2 and 0.20 gL^{-1} NaHCO_3) using a potentiostat (Model 362, EG&G, Instruments, Princeton Applied Research, Princeton, NJ, USA) with a silver chloride electrode (SCE) as the reference electrode. For each specimen, five polarisation curves were obtained under room temperature conditions ($28 \text{ }^\circ\text{C} \pm 1 \text{ }^\circ\text{C}$) using a voltage range of -600 mV to 200 mV and a scan rate of 1 mV/s . To ensure experimental reliability, data collection was under similar conditions and standard deviation is within reasonable range ($\pm 10 \text{ mv}$) the polarisation curve was obtained, and each alloy was tested five times, with a new sample being used on each occasion.

3. Results and Discussion

3.1. XRD Structural Analysis

Figure 1 shows the XRD patterns of the three as-cast specimens. It can be seen that all three samples had a lamellar structure with a mixture of γ and α_2 phase. As the Cu content increased from 3 to 4 at.%, the intensity of the main γ peak decreased, while that of the main α_2 peak increased. However, as the Cu content further increased to 5 at.%, the magnitude of the γ peak increased once again. It has been reported that the presence of the α_2 phase enhances the ductility and strength of TiAl intermetallic alloy, whereas γ phase leads to increased brittleness [34].

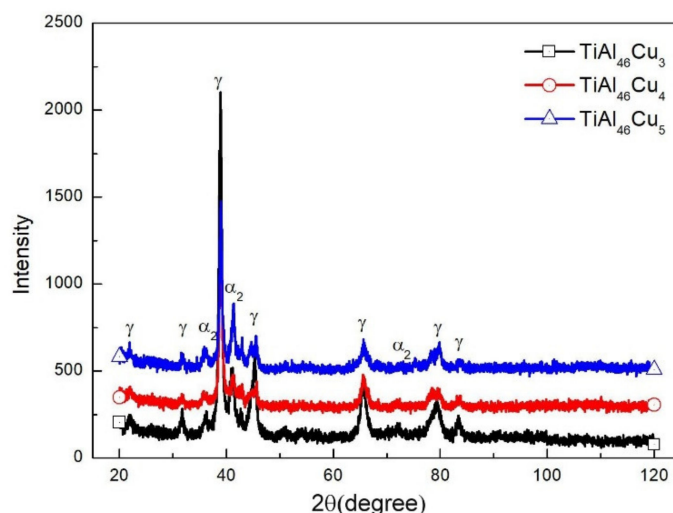


Figure 1. XRD patterns of $\text{TiAl}_{46}\text{Cu}_x$ specimens with $x = 3, 4$ and 5 at.%.

3.2. Stress–Strain Analysis

Figure 2a–c show the stress–strain response of the various TiAlCu_x specimens under quasistatic deformation conditions. For all of the specimens, the flow stress increased at higher strain rates. Moreover, at each strain rate, the maximum stress increased with an increasing strain rate. Overall, however, the results showed that the maximum flow stress was determined mainly by the strain rate. All of the specimens ultimately fractured at high strain values. However, the fracture strain reduced as the strain rate increased (see

Table 1), which suggests that the TiAlCu_x specimens undergo a strengthening effect at higher strain rates. Comparing the various stress–strain curves in Figure 2a–c, it was found that the TiAlCu_x sample with 4 at.% Cu addition had the highest strength and fracture strain among all the samples. In other words, the results confirm the XRD finding above that the TiAl₄₆Cu₄ sample has the best mechanical properties of the considered alloys. The effect of strain rate on the maximum flow stress was more than fracture strain, we can see from Figure 2a or Figure 3a, the maximum flow stress of TiAlCu₃ was increasing from 1500 MPa at strain rate of 10^{-3} s^{-1} to 2100 MPa at strain rate of $4 \times 10^3 \text{ s}^{-1}$. The flow stress was increasing about 600 MPa. Comparing the same specimens for TiAlCu₄ and TiAlCu₅, they were also increasing flow stress of about 500–600 MPa with increasing strain rate from 10^{-3} to $4 \times 10^3 \text{ s}^{-1}$.

Figure 3a–c present the stress–strain curves of the TiAlCu_x specimens tested under dynamic loading conditions. As for the results presented in Figure 2 for the quasistatic loading case, the maximum flow stress increased as the strain rate increased for all of the specimens, while the fracture strain decreased. Furthermore, the specimen with a Cu addition of 4 at.% again possessed the best mechanical properties of the various samples.

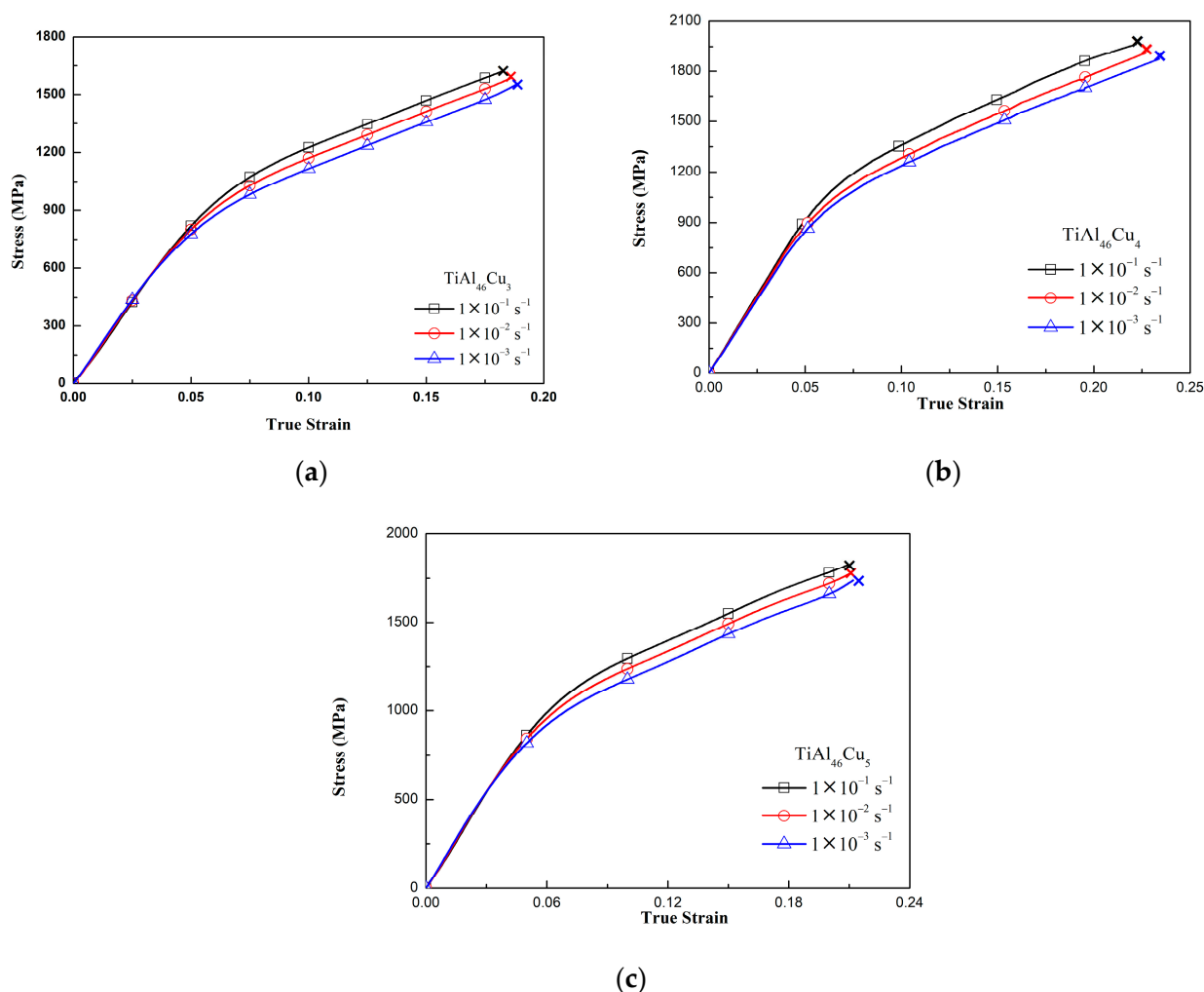


Figure 2. Stress–strain curves of TiAl₄₆Cu_x specimens under quasistatic strain rates: (a) TiAl₄₆Cu₃; (b) TiAl₄₆Cu₄; and (c) TiAl₄₆Cu₅.

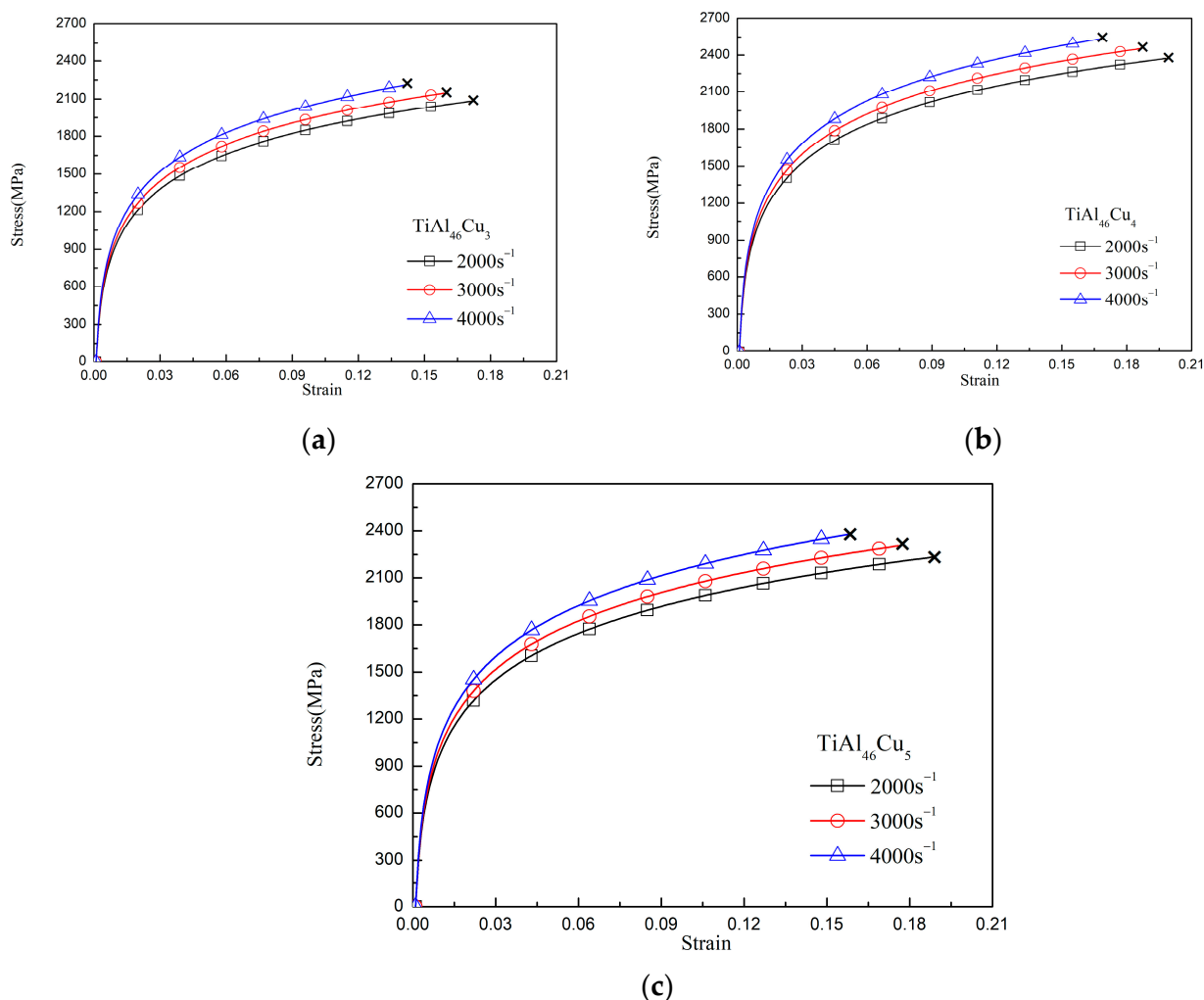


Figure 3. Stress–strain curves of $\text{TiAl}_{46}\text{Cu}_x$ specimens under dynamic strain rates: (a) $\text{TiAl}_{46}\text{Cu}_3$; (b) $\text{TiAl}_{46}\text{Cu}_4$; and (c) $\text{TiAl}_{46}\text{Cu}_5$.

Table 1. The fracture strain for all tested specimens under different strain rates.

	10^{-3}	10^{-2}	10^{-1}	2×10^3	3×10^3	4×10^3
TiAlCu_3	0.195	0.185	0.18	0.17	0.16	0.14
TiAlCu_4	0.24	0.23	0.22	0.2	0.19	0.17
TiAlCu_5	0.22	0.21	0.2	0.19	0.18	0.16

3.3. Strain Rate Effect

In general, Figures 2 and 3 show that the strain rate has a significant effect on the flow response of the TiAlCu_x samples. This effect can be quantified by the strain rate sensitivity factor, β , which is defined as [35]

$$\beta = \partial\sigma / \partial\dot{\epsilon} = (\sigma_2 - \sigma_1) / \ln(\dot{\epsilon}_2 / \dot{\epsilon}_1) \quad (1)$$

where σ_2 and σ_1 are the compressive stresses obtained at average strain rates of $\dot{\epsilon}_2$ and $\dot{\epsilon}_1$, respectively. Figure 4a–c show the variation of β with the strain at different strain rates for the TiAlCu_x samples with Cu additions of 3, 4 and 5 at.%, respectively. It can be seen that for each sample, the strain rate sensitivity increased as the strain and strain rate increased. Furthermore, for a given strain and strain rate, β increased with an increasing Cu content. The effects of the strain rate and Cu content on the strain rate sensitivity reflect the changes in the microstructural evolution of the sample, e.g., the grain size and

precipitate formation. The results in Figure 4 indicate that the TiAlCu_x sample with 4 at.% Cu addition had the highest strain rate sensitivity of all the samples. The results for the strain rate sensitivity in Figure 4 are thus consistent with those for the stress–strain behaviour in Figures 2 and 3. Overall, the results indicate that, while Cu addition enhances the strength of TiAl intermetallic alloy, the level of Cu addition should be controlled to 4 at.% in order to optimize the microstructure and mechanical properties.

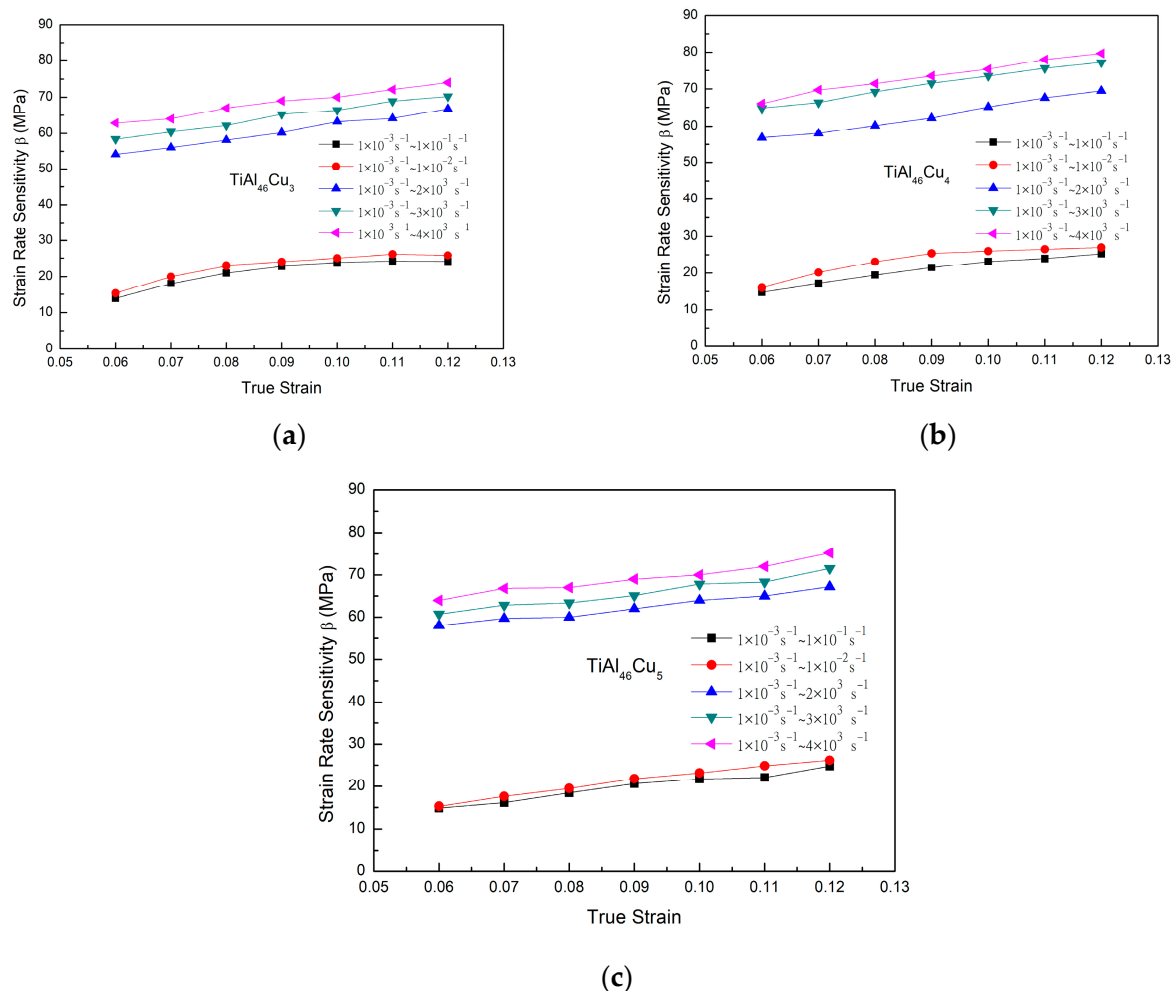


Figure 4. Strain rate sensitivity of $\text{TiAl}_{46}\text{Cu}_x$ specimens under dynamic strain rates: (a) $\text{TiAl}_{46}\text{Cu}_3$; (b) $\text{TiAl}_{46}\text{Cu}_4$; and (c) $\text{TiAl}_{46}\text{Cu}_5$.

3.4. Microstructural Observations and Fracture Analysis

Figure 5a–c present OM images of the matrix microstructures of the as-cast TiAlCu_x specimens with Cu additions of $x = 3\sim 5$ at.%, respectively. It can be seen that the lamellar microstructure ($\gamma + \alpha_2$) became more pronounced with an increasing Cu content. Notably, while a lamellar microstructure enhanced the mechanical strength of TiAl intermetallic alloys, it also increased their brittleness [34]. Figure 6a–f present SEM fractographs of the three TiAlCu_x samples under strain rates of 10^{-3} s^{-1} and $4 \times 10^3 \text{ s}^{-1}$, respectively. As shown in Figure 6a,b, the fracture surface of the TiAlCu_3 specimen contained distinct cleavage-like features characteristic of a brittle fracture mode. Moreover, the number of cleavage features increased at a higher strain rate. It means that the fracture strain decreases when specimens suffer high strain rate deformation. A similar tendency was also observed for the sample containing 4 at.% Cu (see Figure 6c,d). However, the fracture surfaces contained fewer cleavage features than those in Figure 6a,b, and hence it is inferred that the sample has higher ductility than the other two Cu content specimens.

As shown in Figure 6e,f, the fracture surfaces of the specimen with 5 at.% Cu addition contained a large number of cleavage features. In other words, the TiAlCu₅ sample had a brittle characteristic, and thus fractured under a lower flow stress and strain than TiAlCu₄ sample (as shown earlier in Figures 2 and 3).

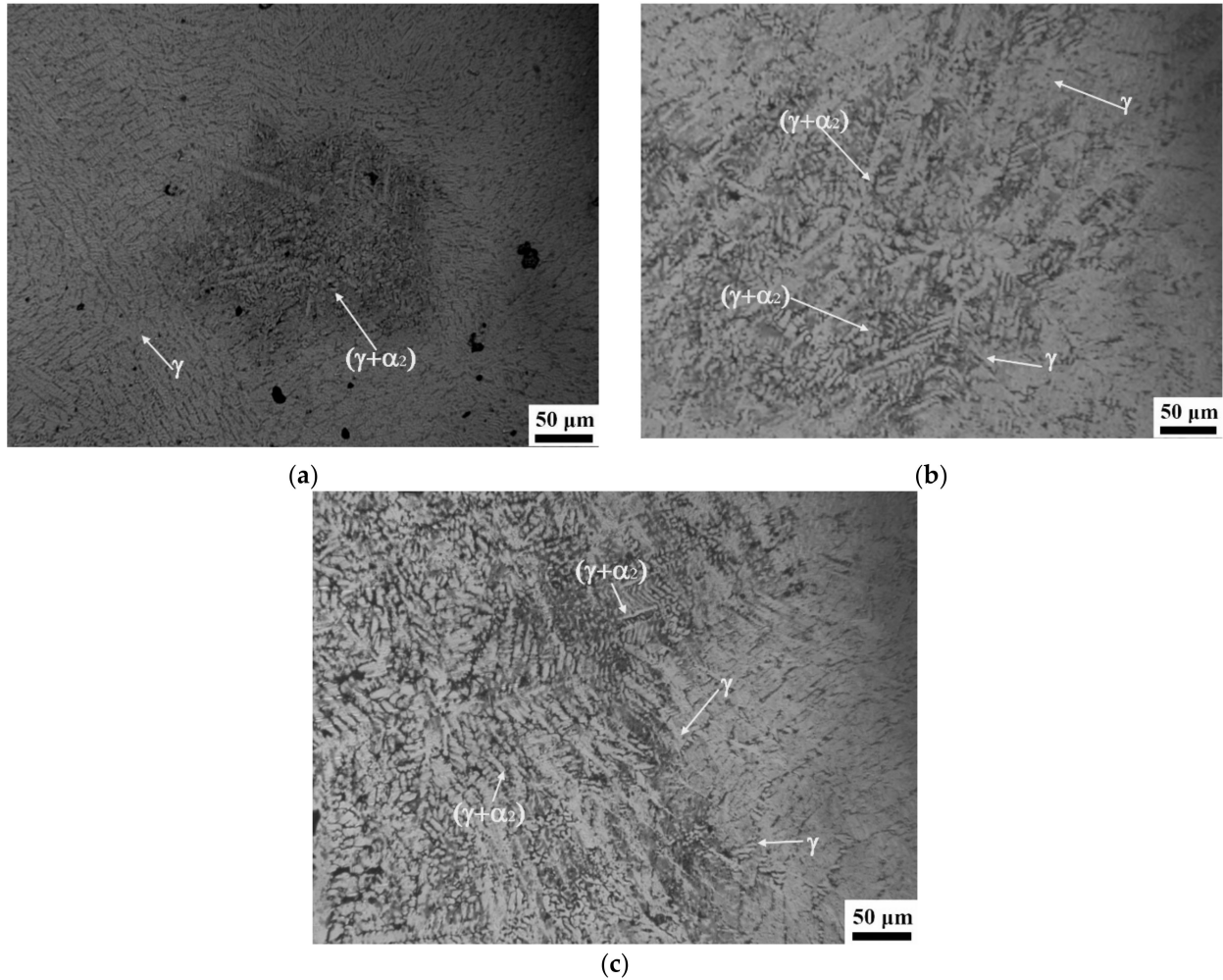


Figure 5. Optical micrographs of as-cast TiAl₄₆Cu_x specimens: (a) TiAl₄₆Cu₃, (b) TiAl₄₆Cu₄, and (c) TiAl₄₆Cu₅.

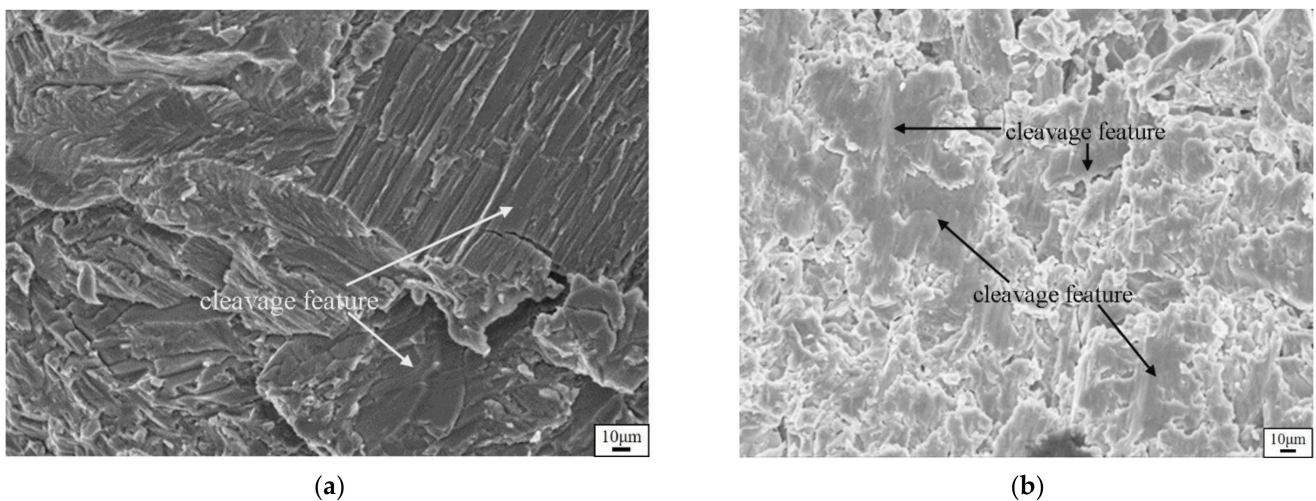


Figure 6. Cont.

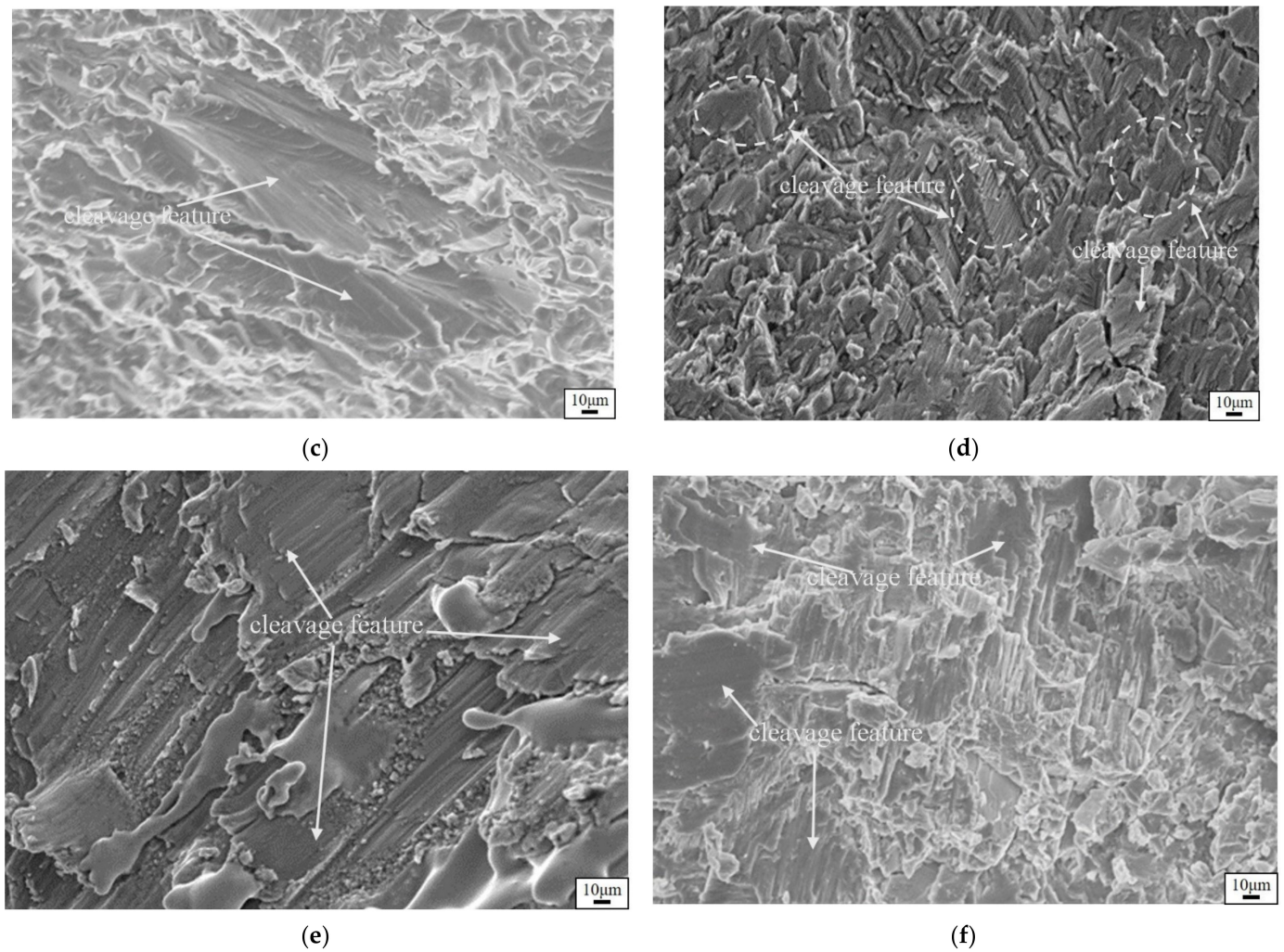


Figure 6. Fracture morphologies of: (a) $\text{TiAl}_{46}\text{Cu}_3$ specimens deformed at $1 \times 10^{-3} \text{ s}^{-1}$, (b) $4 \times 10^{-3} \text{ s}^{-1}$; (c) $\text{TiAl}_{46}\text{Cu}_4$ specimens deformed at $1 \times 10^{-3} \text{ s}^{-1}$, (d) $4 \times 10^{-3} \text{ s}^{-1}$; (e) $\text{TiAl}_{46}\text{Cu}_5$ specimens deformed at $1 \times 10^{-3} \text{ s}^{-1}$, (f) $4 \times 10^{-3} \text{ s}^{-1}$.

3.5. Corrosion Property Analysis

Figure 7 presents the polarisation curves of the as-cast TiAlCu_x specimens. The TiAlCu_x specimen with 4 at.% Cu addition had a corrosion current density, I_{corr} , of approximately $3.5 \times 10^{-8} \text{ A/cm}^2$. By contrast, the specimen with 3 at.% Cu had an I_{corr} value of $5.4 \times 10^{-8} \text{ A/cm}^2$, respectively. In other words, the anti-corrosion performance of the TiAlCu_x sample improved as the Cu addition was increased from 3 to 4 at.%, However, when the Cu content was further increased to 5 at.%, I_{corr} increased to $8.2 \times 10^{-8} \text{ A/cm}^2$. Thus, overall, the results show that the optimal anti-corrosion performance was obtained for the sample with a Cu addition of 4 at.%. It is speculated that the improved anti-corrosion performance is the result of a lower quantity of brittle γ phase and an increased quantity of α_2 phase [34].

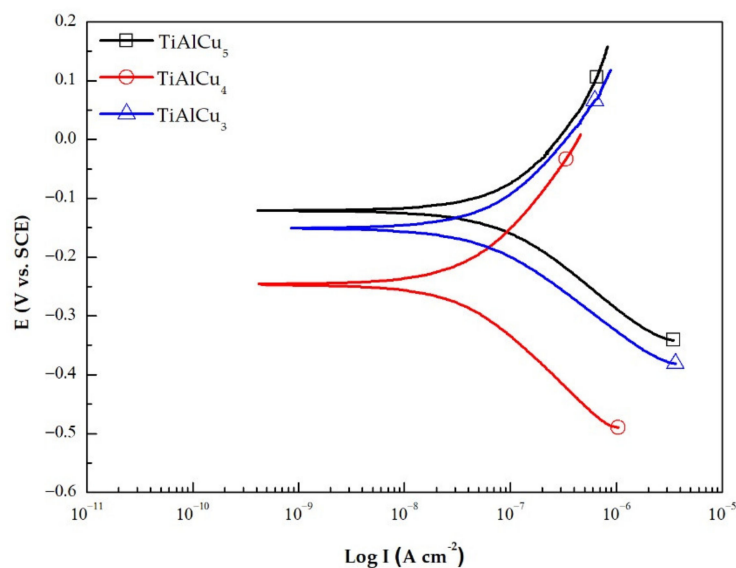


Figure 7. Potentiodynamic polarisation curves of $\text{TiAl}_{46}\text{Cu}_x$ specimens with $x = 3, 4$ and 5 at.%.

4. Conclusions

The results have shown that, for all of the samples, the flow stress and strain rate sensitivity increase at higher strain rates. By contrast, the fracture strain reduces as the strain rate increases. Among all the samples, that with a Cu addition of 4 at.% exhibits the best mechanical response, i.e., a good flow strength and an improved ductility. The microstructural observations have shown that the TiAlCu_x specimens have a lamellar microstructure ($\gamma + \alpha_2$). As the Cu content increases from 3 at.% to 4 at.%, the quantity of brittle γ phase decreases, while that of α_2 phase increases. However, as the Cu content is further increased to 5 at.%, the quantity of γ phase increases once more. The SEM observations showed that the fracture surfaces of all the samples contained distinct cleavage features. The number of cleavage features reduces as the Cu content increases from 3 at.% to 4 at.%, but then increases as the Cu content is increased to 5 at.%. In the electrochemical corrosion tests, the TiAlCu_x sample with 4 at.% Cu addition showed the lowest corrosion current density, I_{corr} . Thus, overall, the results indicate that the TiAlCu_4 sample, with a lower amount of γ phase and higher amount of α_2 phase, has the best mechanical, microstructural and anti-corrosion properties of the considered samples.

Author Contributions: Writing—review, methodology and editing: C.-H.K.; conceptualisation, data analysis and writing—original draft preparation: T.-H.C.; experiment: T.-Y.Z. All authors have read and agreed to the published version of the manuscript.

Funding: This research was funded by the Ministry of Science and Technology of the Republic of China under Grant No. MOST107-2221-E-992-060.

Institutional Review Board Statement: Not applicable.

Informed Consent Statement: Not applicable.

Data Availability Statement: Not applicable.

Acknowledgments: The authors gratefully acknowledge the technical support provided to this study by the National Kaohsiung University of Science and Technology (NKUST).

Conflicts of Interest: The authors declare no conflict of interest.

References

1. Geetha, M.; Singh, A.K.; Asokamani, R.; Gogia, A.K. Ti based biomaterials, the ultimate choice for orthopaedic implants—a review. *Prog. Mater. Sci.* **2009**, *54*, 397–425. [[CrossRef](#)]
2. Long, M.; Rack, H.J. Titanium alloys in total joint replacement—a materials science perspective. *Biomaterials* **1998**, *19*, 1621–1639. [[CrossRef](#)]
3. Yamaguchi, M.; Inui, H. *Structural Intermetallics*; Daloria, R., Lewandowski, J.J., Liu, C.T., Martin, P.L., Miracle, D.B., Nathal, M.V., Eds.; TMS: Warrendale, PA, USA, 1993; p. 127.
4. Yun, J.H.; Oh, M.H.; Nam, S.W.; Wee, D.M.; Inui, H.; Yamaguchi, M. Microalloying effects in TiAl+Mo alloys. *Mater. Sci. Eng. A* **1997**, *239–240*, 702–708. [[CrossRef](#)]
5. Kim, Y.W. Ordered intermetallic alloys, part III: Gamma titanium aluminides. *JOM* **1994**, *46*, 30–39. [[CrossRef](#)]
6. Tetsui, T. Effects of high niobium addition on the mechanical properties and high-temperature deformability of gamma TiAl alloy. *Intermetallics* **2002**, *10*, 239–245. [[CrossRef](#)]
7. Khan, A.S.; Suh, Y.S.; Kazmi, R. Quasi-static and dynamic loading responses and constitutive modeling of titanium alloys. *Int. J. Plast.* **2004**, *20*, 2233–2248. [[CrossRef](#)]
8. Lee, W.S.; Chen, C.W. Dynamic mechanical properties and microstructure of Ti-6Al-7Nb biomedical alloy as function of strain rate. *Mater. Sci. Technol.* **2013**, *29*, 1055–1064. [[CrossRef](#)]
9. Zhan, H.Y.; Wang, G.; Kent, D.; Dargusch, M. The dynamic response of a metastable β Ti–Nb alloy to high strain rates at room and elevated temperatures. *Acta Mater.* **2016**, *105*, 104–113. [[CrossRef](#)]
10. Lee, W.S.; Lin, C.F.; Chen, T.H.; Luo, W.Z. High temperature deformation and fracture behaviour of 316L stainless steel under high strain rate loading. *J. Nucl. Mater.* **2012**, *420*, 226–234. [[CrossRef](#)]
11. Follansbee, P.S.; Kocks, U.F. A constitutive description of the deformation of copper based on the use of the mechanical threshold stress as an internal state variable. *Acta Metall.* **1988**, *36*, 81–93. [[CrossRef](#)]
12. Zerilli, F.J.; Armstrong, R.W. The effect of dislocation drag on the stress-strain behavior of F.C.C. metals. *Acta Metall. Mater.* **1992**, *40*, 1803–1808. [[CrossRef](#)]
13. Som, I.; Balla, V.K.; Das, M.; Sukul, D. Thermally oxidized electron beam melted γ -TiAl: In vitro wear, corrosion, and biocompatibility properties. *J. Mater. Res.* **2018**, *33*, 2096–2105. [[CrossRef](#)]
14. Gogheri, M.S.; Kasiri-Asgarani, M.; Bakhsheshi-Rad, H.R.; Ghayour, H.; Rafiei, M. Mechanical properties, corrosion behavior and biocompatibility of orthopedic pure titanium–magnesium alloy screw prepared by friction welding. *Trans. Nonferrous Met. Soc.* **2020**, *30*, 2952–2966. [[CrossRef](#)]
15. Lopes, C.; Gabor, C.; Cristea, D.; Costa, R.; Domingues, R.P.; Rodrigues, M.S.; Borges, J.; Alves, E.; Barradas, N.P.; Munteanu, D.; et al. Evolution of the mechanical properties of Ti-based intermetallic thin films doped with different metals to be used as biomedical devices. *Appl. Surf. Sci.* **2020**, *505*, 144617. [[CrossRef](#)]
16. Ono, N.; Nowak, R.; Miura, S. Effect of deformation temperature on Hall–Petch relationship registered for polycrystalline magnesium. *Mater. Lett.* **2004**, *58*, 39–43. [[CrossRef](#)]
17. Lee, W.S.; Lin, C.F.; Chen, T.H.; Chen, H.W. Dynamic impact response of inconel 718 alloy under low and high temperatures. *Mater. Trans.* **2011**, *52*, 1734–1740. [[CrossRef](#)]
18. Norfleet, D.M.; Dimiduk, D.M.; Polasik, S.J.; Uchic, M.D.; Mills, M.J. Dislocation structures and their relationship to strength in deformed nickel microcrystals. *Acta Mater.* **2008**, *56*, 2988–3001. [[CrossRef](#)]
19. Jarmakani, H.; McNaney, J.M.; Kad, B.; Orlikowski, D.; Nguyen, J.H.; Meyers, M.A. Dynamic response of single crystalline copper subjected to quasi-isentropic, gas-gun driven loading. *Mater. Sci. Eng. A* **2007**, *463*, 249–262. [[CrossRef](#)]
20. Johnson, G.R.; Cook, W.H. A constitutive model and data for metals subjected to large strains, high strain rates and high temperatures. In Proceedings of the 7th International Symposium on Ballistics, Hague, The Netherlands, 19–21 April 1983; pp. 541–547.
21. Galiyev, A.; Kaibyshev, R.; Gottstein, G. Correlation of plastic deformation and dynamic recrystallization in magnesium alloy ZK60. *Acta Mater.* **2001**, *49*, 1199–1207. [[CrossRef](#)]
22. Zerilli, F.J.; Armstrong, R.W. Dislocation-mechanics-based constitutive relations for material dynamics calculations. *J. Appl. Phys.* **1987**, *61*, 1816–1825. [[CrossRef](#)]
23. Lin, C.W.; Ju, C.P.; Lin, J.-H.C. A comparison of the fatigue behavior of cast Ti-7.5Mo with c.p. titanium, Ti-6Al-4V and Ti-13Nb-13Zr alloys. *Biomaterials* **2005**, *26*, 2899–2907. [[CrossRef](#)]
24. Cvijović-Alagić, I.; Cvijović, Z.; Mitrović, S.; Panić, V.; Rakin, M. Wear and corrosion behaviour of Ti–13Nb–13Zr and Ti–6Al–4V alloys in simulated physiological solution. *Corros. Sci.* **2011**, *53*, 796–808. [[CrossRef](#)]
25. Niinomi, M. Mechanical properties of biomedical titanium alloys. *Mater. Sci. Eng. A* **1998**, *243*, 231–236. [[CrossRef](#)]
26. Ferguson, W.G.; Kumar, A.; Dorn, J.E. Dislocation damping in aluminum at high strain rates. *J. Appl. Phys.* **1967**, *38*, 1863. [[CrossRef](#)]
27. Cabibbo, M.; Knaislová, A.; Novák, P.; Průša, F.; Paoletti, C. Role of Si on lamellar formation and mechanical response of two SPS Ti–15Al–15Si and Ti–10Al–20Si intermetallic alloys. *Intermetallics* **2021**, *131*, 107099. [[CrossRef](#)]
28. Han, J.K.; Li, X.; Dippenaar, R.; Liss, K.D.; Kawasaki, M. Microscopic plastic response in a bulk nano-structured TiAl intermetallic compound processed by high-pressure torsion. *Mater. Sci. Eng. A* **2018**, *714*, 84–92. [[CrossRef](#)]

29. Amirian, B.; Li, H.Y.; Hogan, J.D. The mechanical response of a α_2 (Ti₃Al) + γ (TiAl)-submicron grained Al₂O₃ cermet under dynamic compression: Modeling and experiment. *Acta Mater.* **2019**, *181*, 291–308. [[CrossRef](#)]
30. Anurag, S.; Guo, Y.B. A modified micromechanical approach to determine flow stress of work materials experiencing complex deformation histories in manufacturing processes. *Int. J. Mech. Sci.* **2007**, *49*, 909–918. [[CrossRef](#)]
31. Uenishi, A.; Teodosiu, C. Constitutive modelling of the high strain rate behaviour of interstitial-free steel. *Int. J. Plast.* **2004**, *20*, 915–936. [[CrossRef](#)]
32. Abed, F.H.; Voyiadjis, G.Z. A consistent modified Zerilli-Armstrong flow stress model for BCC and FCC metals for elevated temperatures. *Acta Mech.* **2005**, *175*, 1–18. [[CrossRef](#)]
33. Petch, N.J. The cleavage strength of polycrystals. *J. Iron Steel Inst.* **1953**, *174*, 25–28.
34. Imayev, V.M.; Imayev, R.M.; Salishchev, G.A. On two stages of brittle-to-ductile transition in TiAl intermetallic. *Intermetallics* **2000**, *8*, 1–6. [[CrossRef](#)]
35. Shi, L.; Northwood, D. The mechanical behavior of an AISI type 310 stainless steel. *Acta Metall. Mater.* **1995**, *43*, 453–460. [[CrossRef](#)]